THE JOURNAL OF PHYSICAL CHEMISTRY B

ARTICLE

pubs.acs.org/JPCB

Deuterium Magic Angle Spinning NMR Used To Study the Dynamics of Peptides Adsorbed onto Polystyrene and Functionalized Polystyrene Surfaces

Nicholas F. Breen,[†] Kun Li,[‡] Gregory L. Olsen,[†,§] and Gary P. Drobny*[,†,‡]

[†]Department of Chemistry and [‡]Department of Physics, University of Washington, Seattle, Washington 98195, United States

Supporting Information

ABSTRACT: LKα14 is a 14 amino acid peptide with a periodic sequence of leucine and lysine residues consistent with an amphipathic α-helix. This "hydrophobic periodicity" has been found to result in an α-helical secondary structure at air−water interfaces and on both polar and nonpolar solid polymer surfaces. In this paper, the dynamics of LKα14 peptides, selectively deuterated at a single leucine and adsorbed onto polystyrene and carboxylated polystyrene beads, are studied using ^{2}H magic angle spinning (MAS) solid state NMR over a 100 °C temperature range. We first demonstrate the sensitivity enhancement possible with ^{2}H MAS techniques, which in turn enables us to obtain high-quality ^{2}H NMR spectra for selectively deuterated peptides adsorbed onto solid polymer surfaces. The extensive literature shows that the dynamics of leucine side chains are sensitive to the local structural environment of the protein. Therefore, the degree to which the dynamics of leucine side chains and the backbone of the peptide LKα14 are influenced by surface proximity and surface chemistry is studied as a function of temperature with ^{2}H MAS NMR. It is found that the dynamics of the leucine side chains in LKα14 depend strongly upon the orientation of the polymer on the surface, which in turn depends on whether the LKα14 peptide adsorbs onto a polar or nonpolar surface. ^{2}H MAS line shapes therefore permit probes of surface orientation over a wide temperature range.

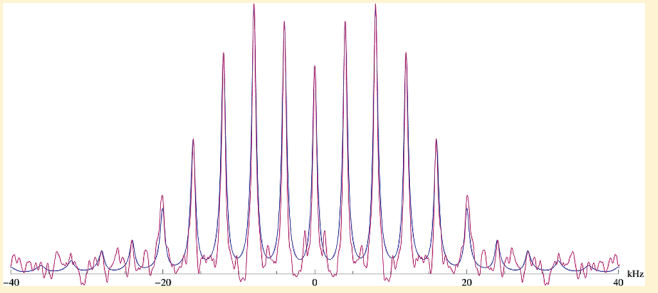

INTRODUCTION

Deuterium solid state nuclear magnetic resonance (^{2}H NMR) is a versatile, nonperturbing, quantitative probe of biopolymer dynamics over a broad range of motional rates. The solid state ^{2}H NMR spectrum is dominated by the interaction of the electric quadrupole moment of the deuterium nucleus with surrounding electric field gradients. The magnitude of this interaction is quantified by the deuterium quadrupolar coupling constant (i.e., QCC = $3e^2qQ/4\hbar$), which is on the order of 170 kHz for deuterons in sp^3 hybridized carbon−deuterium bonds.[1] Given the magnitude of the anisotropy of the deuterium quadrupolar interaction, the dynamic regimes probed by ^{2}H NMR are by convention divided into (1) very fast motions (correlation time τ_C < 100 ns), which induce relaxation; (2) fast motions (τ_C < 10 μs), which partially average the anisotropy of the quadrupolar interaction; (3) intermediate motions with rates on the order of the anisotropy of the quadrupolar interaction (10 μs < τ_C < 1 ms), which dynamically perturb ^{2}H NMR line shapes; and (4) slow motions (1 ms < τ_C), which are probed by studies of the rate of decay of ^{2}H spin alignment.[2]

^{2}H NMR line shapes obtained with a quadrupolar echo pulse sequence are extremely sensitive to dynamic amplitudes and dynamic rates in the 10^4−10^7 Hz range,[3−6] whereas spin−lattice relaxation studies can probe very fast motions. Although quadrupolar echo line shapes and partially relaxed line shapes have been used to quantify molecular samples with high deuterium enrichment levels, ^{2}H NMR has practical limitations. For example, the relatively large anisotropy of the quadrupolar interaction results in very broad, heterogeneous line shapes for polycrystalline samples, which together with the small magnetic moment of the deuterium nucleus results in low sensitivity. For this reason, application of ^{2}H NMR to magnetically dilute samples, including selectively deuterated proteins and nucleic acids, is challenging. For example, in composite systems consisting of selectively deuterated proteins associated with lipid bilayers[7] or adsorbed onto material surfaces,[8] further dilution of the deuterated sample content occurs, and the application of ^{2}H NMR spectroscopy becomes even more challenging.

Deuterium magic angle spinning (^{2}H MAS) NMR has emerged in recent years as a viable alternative to static quadrupolar echo spectroscopy.[9−12] Spinning a deuterated sample rapidly around an axis that is oriented at 54.74° (i.e., the magic angle) relative to the direction of the static external magnetic field averages the ^{2}H NMR solid state line shape into an isotropic resonance and side

Received: October 25, 2010
Revised: June 7, 2011
Published: June 08, 2011

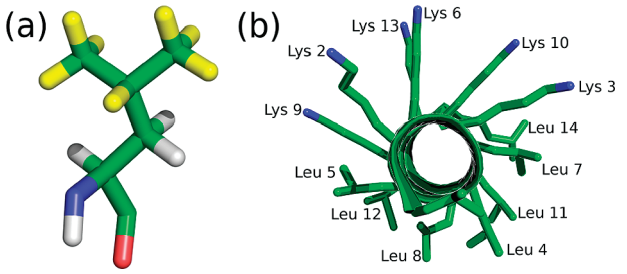

Figure 1. (a) Structure of leucine, with deuterated sites identified in yellow. (b) Side chain orientations of the residues in LKα14.

bands separated by intervals of the spinning frequency, ν_R, where typically 1 kHz < ν_R < 20 kHz. Because the integrated intensity of the ^{2}H NMR spectrum is concentrated into a small number of resonances in a MAS experiment, sensitivity enhancements of 20−30 are easily achievable. This feature makes ^{2}H MAS NMR a potentially powerful approach for studying the dynamics of very small quantities of selectively deuterated biopolymers adsorbed onto biomaterial surfaces.

This paper has two purposes. First, we describe the application of ^{2}H MAS NMR to the study of the dynamics of a selectively deuterated peptide adsorbed onto a nonpolar polystyrene surface and a polar surface obtained by carboxylating polystyrene. Second, using an in-house program, KLDMAS, to simulate dynamically averaged ^{2}H NMR line shapes, we present a quantitative analysis of these side chain motions. The degree to which peptide dynamics reflect the orientation of the surface-adsorbed peptide on differently functionalized polymer surfaces is investigated over a 100 °C temperature range.

We chose for study the 14-amino acid "LK" peptide composed of alternating periods of leucine (L) and lysine (K) residues,[13] the so-called LKα14 peptide: Ac-LKKLLKLLKKLLKL−OH where L-leucine-isopropyl-$^2H_7$ (d_7Leu) was incorporated at the L8 position. See Figure 1a. Degrado and Lear first demonstrated that short peptides possessing "hydrophobic periodicity" (i.e., matching that of amphiphilic α-helices) adopt a structure and orientation at hydrophobic surfaces, to sequester hydrophobic residues in a favorable environment rather than remaining in an unfolded state, as observed in aqueous solution. Previously, we have used ^{13}C dipolar recoupling solid state NMR to quantify the local α-helical structure of selectively ^{13}C-labeled LKα14 peptide adsorbed onto polystyrene (PS) bead surfaces.[14] Structured as an α-helix on PS bead surfaces, LKα14 is amphipathic, with one-half of the cylinder surface dominated by nonpolar leucine side chains and the other half dominated by positively charged lysine side chains. See Figure 1b. The interactions of LKα14 with PS and silica surfaces have been studied also by Somorjai and co-workers,[15,16] who used sum frequency generation (SFG) vibrational spectroscopy to show that LKα14 adsorbs onto PS with the leucine side chains alongside and lysine side chains opposite the surface, whereas the opposite orientation occurs on negatively charged silica surfaces. In both cases, SFG spectroscopy found, as did solid state NMR, that surface-adsorbed LKα14 is structured as an α-helix.

We have also used SFG and ^{2}H NMR conjointly to study both the leucine side chain dynamics and the surface orientation for LKα14 adsorbed onto PS surfaces and onto colloidal gold particles coated with a self-assembled monolayer of carboxylated alkane thiolates.[8,17] In those works, trends in ^{2}H NMR static line shapes were shown to be correlated with the orientation of the leucine side chain relative to the PS surface, as determined by SFG. For L8 in particular, SFG studies of LKα14 selectively deuterated at individual leucines and adsorbed onto PS and showed that the $C_\alpha-C_\beta$ bond of L8 is nearly parallel to the PS surface normal.[16] The isopropyl group of L8 is therefore very likely in close proximity to the PS surface but more remote from the carboxylated polystyrene (PSCOOH) surface.

Here, we apply ^{2}H MAS spectroscopic techniques to study the side chain dynamics of leucyl peptides adsorbed onto functionalized polymer surfaces as a function of temperature and surface chemistry. Because of its varying proximity to PS and PSCOOH surfaces, we investigate the degree to which ^{2}H MAS line shapes isopropyl-deuterated L8 in LKα14 vary in response to a change in temperature and surface chemistry. In particular, the detailed nature of the peptide side chain motions on PS and PSCOOH surfaces is extracted from an analysis of the ^{2}H MAS line shape and spin−lattice relaxation rates over a 100 °C temperature range. The overall intent is to determine the degree to which amino acid side chain dynamics as elucidated by ^{2}H MAS NMR are diagnostic of surface orientation and surface proximity. In addition, the degree to which peptide side chain dynamics at a material interface resembles side chain dynamics in other contexts (i.e. in the hydrophobic interior of folded proteins or inserted into lipid bilayers) is discussed. We also briefly describe in-house software LKDMAS, developed for the purpose of simulating dynamically modulated ^{2}H MAS line shapes.

MATERIALS AND METHODS

Peptide Synthesis and Characterization. L-Leucine, isopropyl-$^2H_7$ (99% atom ^{2}H) was purchased from Cambridge Isotope Laboratories (Andover, MA) and Fmoc-protected using standard protocols.[18] Natural abundance amino acids were purchased in protected form from Novabiochem and used directly. Peptides were synthesized on a Rainin PS3 automated synthesizer using Wang resin and NMP solvent. After resin cleavage and lyophilization, sample purity was confirmed with mass spectroscopy. The peptide did not require further purification.

Peptide Adsorption to Polystyrene and NMR Sample Preparation. Peptides were adsorbed to polystyrene by adding 1.55 mg of peptide (in aqueous solution at 5.0 mg/mL) to 3 mL of an aqueous suspension of 1.0-μm-diameter polystyrene beads (Polysciences) and 40 mL of 0.13× PBS buffer at pH 7.0. The mixture was stirred gently at room temperature for 4 h, then centrifuged for 2 h at 3000*g*. The supernatant was decanted off, and the pellet was again suspended in ∼1 mL of deuterium-depleted water and centrifuged at 10000*g* for 10 min. This washing step was repeated twice more, following which the final resuspension was flash-frozen and lyophilized for 5 days. UV analysis of the supernatant indicated 85−90% peptide binding.

^{2}H NMR Experiments. All static quadrupolar echo experiments were performed at 17.6 T field (115.14 MHz deuterium Larmor frequency) using a home-built, single-channel, static deuterium probe with a Bruker Avance II spectrometer and a 90° pulse time of 2.65 μs. Samples consisted of 40 mg of bead/peptide powder contained in a Kel-F sample holder. All measurements were made at room temperature (∼23 °C). A quadrupolar echo pulse sequence,[19] in which the second half of the echo signal was acquired and Fourier-transformed following left-shift of all time-domain data sets to their respective echo maxima, was used to obtain line shapes. Quadrupolar echo experiments used eight-step phase cycling, with an echo delay of 40 μs. Typical spectra

resulted from acquisition of 360 000−400 000 transients at a recycle delay of 0.35 s. Lineshapes were minimally processed with 1 kHz line broadening and phase correction only.

MAS line shapes were acquired at a deuterium Larmor frequency of 61.38 MHz using a Varian T3MAS probe, 4 mm sample rotors packed with 30 mg of sample, and a home-built spectrometer. These experiments employed a single ^{2}H 90° pulse width of 3.2 μs. Spectra were acquired at spinning speeds of 4000 Hz. LKα14 samples adsorbed onto polystyrene or carboxylated polystyrene surfaces were signal-averaged for 530 000 scans. Inversion recovery spectra were acquired from the same sample rotors at a frequency of 76.75 MHz using a 6.0 μs 180° inversion pulse followed by a variable delay and a 3.0 μs, 90°, quadrupolar echo pulse. Samples were spun at 5000 Hz and signal-averaged with 120 000 scans per time point. After left-shifting to the peak of the first echo, FIDs were Fourier transformed and phase-corrected without further processing.

CALCULATIONS

^{2}H Static and MAS Line Shape Simulations. Quadrupolar echo spectra were simulated numerically with MXET1.[14] ^{2}H NMR MAS spectra and inversion−recovery experiments were simulated with an in-house program, KLDMAS. Here we describe briefly the theoretical approach used by KLDMAS. Simulation of the static ^{2}H quadrupolar line shape is accomplished by Fourier transformation of the calculated response of a system of deuterium spins to a 90° pulse. Calculation of the spin system response, in turn, requires integration of the Liouville equation:

$$\frac{dM_{\pm}}{dt} = \Gamma M_{\pm}(t) = (i\omega_{\pm} + \pi)\, M_{\pm}(t) \qquad (1)$$

where $M(t)$ is the transverse magnetization, the subscript $\pm$ refers to the $m = 1$ to $m = 0$ or the $m = 0$ to $m = -1$ transition, π is the matrix that describes the process of exchange between n discrete conformational sites, and $\omega_{\pm}$ is a diagonal matrix with nonzero diagonal elements corresponding to the resonance frequencies of the deuterium spin at the various sites:

$$\omega_{\pm}^{j} = \pm \frac{3e^2qQ}{4\hbar}\left[\sum_{a=-2}^{+2} D_{0a}^{(2)}\left(\Omega_j^{PC}\right) D_{a0}^{(2)}\left(\Omega^{CL}\right)\right] \qquad (2)$$

In eq 2, all symbols have their usual meanings.[20−22] $\Omega_j^{PC} = (\varphi_j, \theta_j, 0)$ is the solid angle that relates the principal axis system (P) of the (axial) EFG tensor at the jth site relative to the C frame, wherein is fixed the dynamic axis. Ω^{CL} similarly relates the C frame to the laboratory frame (L). Equation 1 can be easily integrated to obtain:

$$M_{\pm}(t) = I \cdot T \cdot e^{\lambda t} \cdot T^{-1} \cdot M_{\pm}(0) \qquad (3)$$

where I is the vector composed of ones, λ is a diagonal matrix whose nonzero elements are the complex eigenvalues of $i\omega_{\pm} + \pi$, T is the matrix whose columns are the eigenvectors of $i\omega_{\pm} + \pi$, and $M_{\pm}(0)$ is the vector describing the initial state of the spin system. The NMR line shape is obtained as a "powder average" of the Fourier transform of eq 3 over all possible orientations of the C frame relative to the L frame.

A similar analysis applies to the response of the spin system to a quadrupolar echo pulse sequence.[20] For a spin 1 system to which two 90° pulses are applied with mutual phase difference of $\pi/2$ and separated by a time τ_1, the response after a time τ_2 following the second 90° pulse is

$$M_{\pm}(t) = 1 \cdot T \cdot e^{\lambda(t+\tau_2)} \cdot T^{-1} \cdot S \cdot e^{\kappa\tau_1} \cdot S^{-1} \cdot M_{\pm}(0) \qquad (4)$$

All symbols in eq 4 are defined as in eq 3, in addition to which κ is the matrix of eigenvalues of $-i\omega_{\pm} + \pi$, and S is the corresponding matrix of eigenvectors.

In a MAS experiment, a powdered sample is spun at a frequency ν_R around a goniometer whose axis is tilted at 54.74 degrees relative to the direction of the static magnetic field. This rotation imparts a time dependence to the elements of the matrix $\omega_{\pm}$, shown in eq 2 for the nonrotating case. For the MAS experiment, eq 1 becomes

$$\frac{dM_{\pm}}{dt} = \Gamma(t)\, M_{\pm}(t) = \left(i\omega_{\pm}(t) + \pi\right) M_{\pm}(t) \qquad (5)$$

Because of the time dependence of $\omega_{\pm}$, eq 5 cannot be integrated to the form of eq 3 by the simple process described above. There are two approaches for accomplishing such an integration. Because eq 5 has the form of an ordinary differential equation with periodic coefficients, in the sense that $\omega_{\pm}(t + \tau_R) = \omega_{\pm}(t)$ where τ_R is the rotor period, Floquet's theorem is applicable.[23] This means that a coordinate change can be found that converts eq 5 to a differential equation with constant coefficients. Floquet's theorem has been used to analyze various periodic motion problems in NMR, including dynamic MAS line shapes[24] and homonuclear and heteronuclear dipolar recoupling experiments,[24] and it is the basis for the dynamic line shape simulation program EXPRESS by Vold and Hoatson.[12]

Another approach, developed by Duer and Levitt,[25] is to numerically integrate eq 5 by dividing the rotor period into N intervals, each of length $\Delta t = \tau_R/N$, where N is sufficiently large that during Δt, $\omega_{\pm}$ and, thus, Γ are approximately constant. Therefore, at any time, $m\Delta t$ (i.e., $1 \le m \le N$), the MAS propagator, can be obtained iteratively:

$$exp(\Gamma(m\Delta t)) \approx exp((i\omega_{\pm}(t_m) + \pi)\Delta t) \times exp(\Gamma((m-1)\Delta t)) \qquad (6)$$

where $t_m = (m - 1)\Delta t/2$ and we assume $\Gamma(0) = 1$. The propagator for any time $t + M\tau_R$ is then given by

$$exp(\Gamma(t + M\tau_R)) \approx \left(exp(\Gamma(\tau_R))\right)^M \times exp(\Gamma(t)) \qquad (7)$$

Equations 6 and 7 are the basis for our ^{2}H MAS line shape simulation program KLDMAS, which was used to generate all MAS line shape simulations shown in this paper.

KLDMAS is also used in this paper to simulate inversion−recovery MAS experiments. The response of the deuterium spin system to an inversion−recovery pulse sequence is obtained by multiplying the iterated propagator by $(1 - 2e^{-\tau/\langle T_1\rangle})$ where τ is the variable time delay between the inversion pulse and the 90° pulse, and the spin−lattice relaxation rate $R_1 = 1/T_1$ is given by

$$R_1 = 1/T_1 = \frac{3}{16}\left(\frac{e^2qQ}{\hbar}\right)^2 \cdot [J_1(\omega) + 4J_2(2\omega)] \qquad (8)$$

In the limit that the rate of spinning exceeds the static spin−lattice relaxation rate and for the case of exchange among N discrete

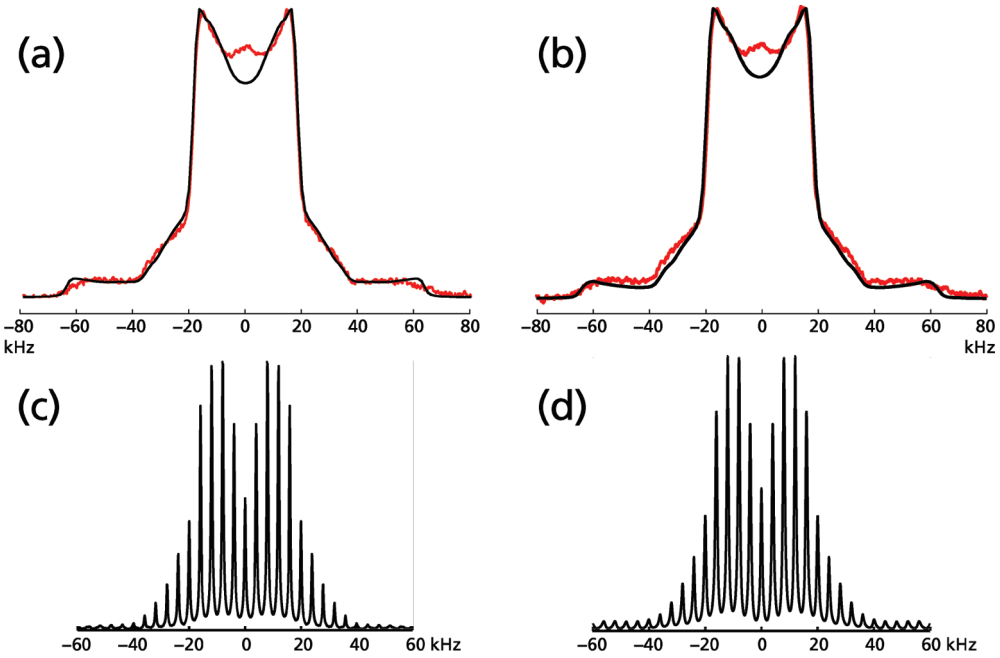

Figure 2. (a, b) Red lines, experimental ^{2}H static NMR line shapes (identical in both); black lines, simulation fits using (a) parameter set 1 and (b) set 2. (c) MAS line shape of unbound LKα14, deuterated at Leu8. (d) Simulation of data in part c using parameter set 1.

sites, the spectral density has the form:[26]

$$J_m(\omega) = 2\int_0^\infty \bar{C}_m(t)\, cos(\omega t)\, dt$$

$$= \sum_{b=-2}^{2} \left[d^{(2)}_{mb}(\theta_{lm})\right]^2 \sum_{a,a'=-2}^{2} D^{(2)*}_{ba}(0,\theta_{mc},\psi_{mc})$$

$$D^{(2)}_{ba'}(0,\theta_{mc},\psi_{mc}) \sum_{nlj=0}^{N-1} X^{(0)}_l X^{(n)}_l X^{(0)}_j X^{(n)}_j D^{(2)*}_{a0}(\phi_l,\theta_l,0)$$

$$D^{(2)}_{a'0}(\phi_j,\theta_j,0)\frac{-2\lambda_n}{{\lambda_n}^2+{\omega_0}^2} \qquad (9)$$

In eq 9, the solid angle $\Omega_{LM} = (0, \theta_{lm}, \psi_{lm}(t))$ relates the goniometer frame M to the laboratory frame L. The angle between the magnetic field direction and the goniometer axis is θ_{lm}, and the angle $\psi_{lm}(t) = \omega_r t$ is time-dependent as a result of the sample rotation at a frequency ω_r. The spectral density in eq 9 is therefore the cosine Fourier transform of a correlation function $\bar{C}_m(t)$ that has been averaged over the motion of the spinner. Also in eq 9, X and λ indicate the eigenvector and (diagonal) eigenvalue matrices, respectively, of the symmetrized jump matrix.

RESULTS AND ANALYSIS

Static and MAS Line Shapes. As a basis for comparison to surface-bound peptide data and to determine the degree to which both static and MAS spectra can be fit to the same dynamic model, we first performed a comparative study of the ^{2}H quadrupolar echo and ^{2}H MAS spectra of unbound LKα14. In Figure 2a, b is shown the experimental ^{2}H quadrupolar echo spectrum of unbound LKα14 with Leu-d_7 incorporated at position L8 and acquired at $T = 20$ °C. The static line shape in Figure 2a, b is narrowed as a result of the rapid rotation of the CD_3 groups. Because of its fast rate, this physical motion can be accurately treated in line shape simulations as a "pre-averaged" EFG tensor, where the "effective" quadrupolar coupling constant is reduced from ∼170 kHz to 50 kHz or less. There is also a contribution to the line shape arising from the γ-methine deuteron ($^2H_\gamma$) of the isopropyl group, which retains a QCC of 170 kHz. The larger anisotropy of the γ-methine deuteron together with the fact that the methyl-to-methine deuteron ratio is 6:1 means the ^{2}H static spectrum will be largely dominated by the methyl deuterons. The central portion of the γ-methine deuteron spectrum appears as a rise in the baseline in Figure 2a, b.

If the only dynamics present in the isopropyl group of L8 were the fast CD_3 rotational motion, the ^{2}H spectrum of the CD_3 groups of LKα14 would have the appearance of a narrowed Pake doublet.[27] The deviation of the LKα14 ^{2}H NMR spectrum from the Pake doublet line shape indicates the presence of additional motions of the leucine side chain as well as possible motions of the peptide backbone at intermediate time scales. To account for the other features in Figure 2a, we must consider explicit models for leucine side chain motions.

^{2}H NMR has been used to study leucine side chain dynamics in protein fibrils,[28] hydrated solid proteins,[29−31] and peptides and proteins embedded in lipid bilayers.[32] Combining the three rotational isomers for each of the $C_\alpha-C_\beta$ and $C_\beta-C_\gamma$ bonds, there are nine side chain conformers. Discounting other side chain motions, bond rotational motions conspire to direct the $C_\gamma-C_\delta$ bond in four directions defined by the corners of a tetrahedron.[31] Previous models for the side chain motion typically include exchanges between some or all of these conformers. For example, the early ^{2}H NMR study of uniformly leucine-deuterated helical collagen fibrils by Batchelder et al.[28] used a two-conformer model selecting the orientations observed to be dominant in leucyl-peptide crystal structures: tg^+ and g^-t, where g^+, g^-, and t indicate the gauche +, gauche −, and trans rotational isomers of the $C_\alpha-C_\beta$ and $C_\beta-C_\gamma$ bonds, respectively.[33,34] Using this model and assuming equal a priori populations Batchelder et al. interpreted changes in the ^{2}H line

dx.doi.org/10.1021/jp1101829 |J. Phys. Chem. B 2011, 115, 9452–9460

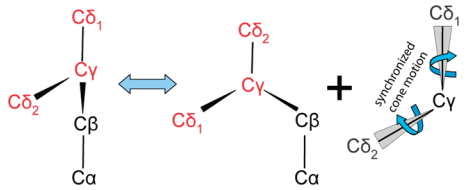

Figure 3. Dynamic model used for ^{2}H NMR simulations.

shape with sample temperature as resulting from changes in the rate of exchange. Separate motion of the peptide backbone was treated by Lorigan in a study of selectively methyl-deuterated phospholamban,[32] a 52-residue transmembrane protein, by incorporating an additional two-site motion around the $C_\beta-C_\gamma$ bond axis, tilting the methyl groups at 75° and jumping in increments of 109.5°. A recent study of the chicken villin headpiece domain HP-36 with a single methyl-deuterated leucine conducted by Vugmeyster et al.[31] successfully extended both approaches: including all four unique conformers with exchange rates in an adjustable ratio of x:1:1:1 and generalizing the backbone motion as a diffusion along an arc at a fixed 70.5° tilt.

To fit the static ^{2}H quadrupolar echo and the ^{2}H MAS spectra for free (i.e., unbound) LKα14 deuterated at L8 shown in Figure 2, we constructed a hybrid model that incorporates elements derived from several models of leucine side chain motion, discussed above. As shown in Figure 3, for the purpose of calculating the MAS line shape, the rapid rotational motions of the CD_3 groups are treated simply with an effective QCC. Rotation of the methyl group is explicitly included as a three-site jump in later calculations of inversion–recovery MAS line shapes. Following Batchelder et al., we use a two-site exchange between the tg^+ and g^-t side chain conformers, corresponding to an angular change of ~109.5° for the $C_\gamma-C_\delta$ bond axis. But as in Vugmeyster et al., we assumed exchange occurs between side chain conformers with unequal a priori populations; that is, essentially a x:y:0:0 model, where $y = 1 - x$. Therefore, the equilibrium site population ratio and thus the ratio of the forward and reverse exchange rate constants k_{12} and k_{21} is an adjustable parameter. These parameters are related by the equilibrium condition

$$k_{12}p_2^{eq} = k_{21}p_1^{eq} \tag{10}$$

Also as in Vugmeyster et al., we rendered the effect of peptide backbone motions as a diffusive motion of the $C_\gamma-C_\delta$ bonds along the arc of a cone. Adjustable parameters for this aspect of the model include the cone half angle and the correlation time associated with the diffusive motion of the $C_\gamma-C_\delta$ bonds on the cone arc.

Given that the CD_3 rotation is treated in line shape calculations with an effective or preaveraged QCC, the motional model used in line shape calculations is explicitly described with two dynamic axes, one of which accounts for the exchange motions of the leucine side chain, and the other accounts for backbone motions of the protein that move the entire amino acid residue. The matrix elements $\omega_\pm(t)$ in eq 5 now assume the form

$$\omega_\pm^{jk}(t) = \pm\left\langle\frac{3e^2qQ}{4\hbar}\right\rangle\sum_{a,b,c=-2}^{2} D_{0a}^{(2)}(\Omega_{LM}(t))^*D_{ab}^{(2)}(\Omega_{MC})^*$$
$$D_{bc}^{(2)}(\Omega_{CI}^k)^*D_{c0}^{(2)}(\Omega_{IP}^j) = \pm\left\langle\frac{3e^2qQ}{4\hbar}\right\rangle\sum_{a,b,c=-2}^{2}$$
$$D_{0a}^{(2)}(0,\theta_{magic},\omega_r t)\,D_{ab}^{(2)}(\alpha,\beta,\gamma)\,D_{bc}^{(2)}(\phi_1^k,\theta_1,\psi_1)$$
$$D_{c0}^{(2)}(\phi_2^j,\theta_2,\psi_2 = 0) \tag{11}$$

Table 1. Parameter Sets 1 and 2 Used To Fit the Static ^{2}H NMR Spectra of Unbound LKα14 Deuterated on the Isopropyl Group of L8, Shown in Figures 3a and b, respectively[a]

parameter	static parameter set 1	static parameter set 2
population ratio p_1/p_2	0.2/0.8	0.2/0.8
k_{12} (s^{-1})	3×10^6	8×10^5
k_{cone} (s^{-1})	800	800
cone half angle (°)	35	25
$\langle QCC\rangle_{eff}$ (kHz)	49.5	50.5
% $^2H_\gamma$	4	6

[a] Parameter set 1 was used to fit the experimental ^{2}H MAS experimental spectrum in Figure 2c. Figure 2d is the MAS simulation using parameter set 1. See text for description of model.

The brackets $\langle\,\rangle$ in eq 11 indicate preaveraging of the quadrupolar coupling constant as a result of the fast methyl group rotation, which, as mentioned above, effectively reduces the QCC from 170 to about 50 kHz. The solid angle $\Omega_{IP}^j = (\varphi_2^j, \theta_2, \psi_2)$ relates the principal axis system of the EFG tensor (P) to the I frame, which is associated with the 2-fold motion of the $C_\gamma-C_\delta$ bonds, with θ_1, in turn describing the $C_\gamma-C_\delta-D$ angle. The angles $\varphi_1^j = 2\pi/3^*(j-1)$ and $\psi_1^j = 2\pi/3^*(j-1)$ represent the side chain conformer site being occupied, where $j = \{1, 2\}$ indicates the site. The solid angle $\Omega_{CI}^k = (\varphi_1^k, \theta_1, \psi_1)$ relates frame I to the crystal frame C, which is fixed to the amino acid framework and within which the local molecular motion is defined. This motion is simulated as a four-site jump of the $C_\gamma-C_\delta$ bonds on the surface of a cone of half angle θ_2, where the site on the cone is specified by $\varphi_2^k = \pi/2(k-1)$, $k = \{1, 2, 3, 4\}$. The z axis of the P frame is assumed to be collinear with the $C_\delta-D$ bond axis, and the EFG tensor is assumed to be axial, which means ψ_2 may be set to zero.

Table 1 summarizes two model parameter sets used to obtain static quadrupolar echo line shape simulations with MXET1 and MAS line shape simulations with KLDMAS, based on the dynamic model shown in Figure 3. Parameter set 1 was used to obtain the simulation of the static quadrupolar echo spectrum shown in Figure 2a superimposed on the experimental spectrum and the MAS spectral simulation shown in Figure 2c. In this parameter set, the population ratio between the two side chain rotational isomers is 0.2/0.8 = 1/4. The kinetic rate constant k_{12} associated with this site exchange is 3×10^6 s^{-1}. The constant k_{21} can be computed given k_{12}, and the population ratio, using eq 10. As mentioned above, the isopropyl group also undergoes a slow gyration, with the $C_\gamma-C_{\delta 1,2}$ bonds moving over the surface of a cone of half angle 35°, modeled as a four-site jump, with equal a priori probabilities and a site-to-site jump rate constant, k_{cone}, of 800 Hz, which is inversely related to the correlation time for diffusion on the cone. The ratio of the γ-methine spectral intensity to the total methyl intensity is ~0.04. The actual molar ratio is ~0.16, and the disparity is attributed to a longer γ-methine T_1, which attenuates the methine signal relative to the CD_3 signal upon extensive signal averaging.

Agreement between the MAS simulation in Figure 2d and MAS data shown in Figure 2c is excellent using parameter set 1, but the simulated ^{2}H static quadrupolar echo spectrum obtained with this parameter set and shown in Figure 2a, does not fit well to the central portion of the experimental spectrum. This is an especially difficult region of the ^{2}H NMR spectrum to fit because residual HDO adsorbed onto the peptide will contribute to the experimental spectrum in this region. If the small peak in the

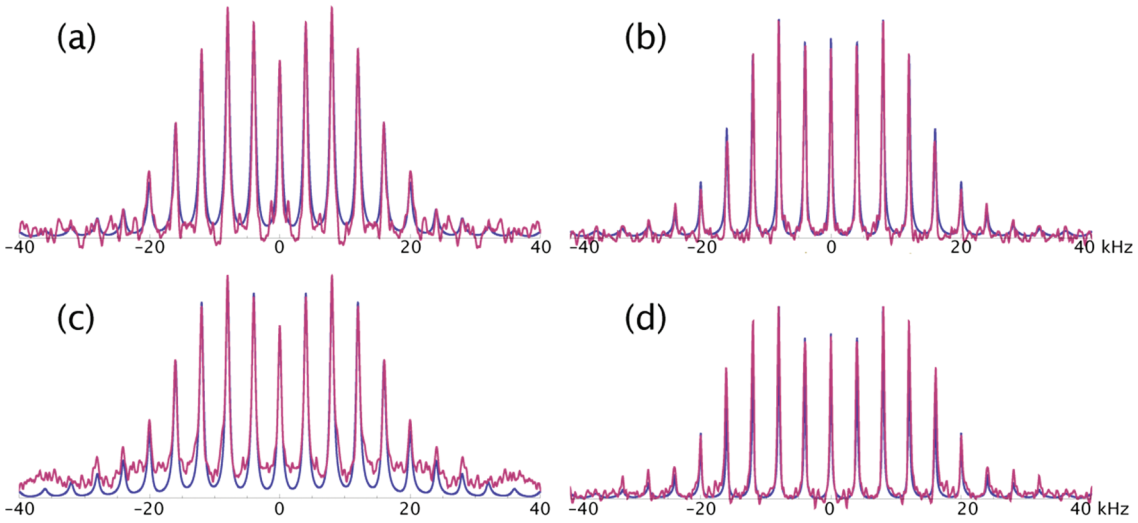

Figure 4. MAS spinning line shapes (purple) and simulation fits (blue) for the L8 peptide at 20 °C on PS (a) and PSCOOH (b) and at −20 °C on PS (c) and PSCOOH (d).

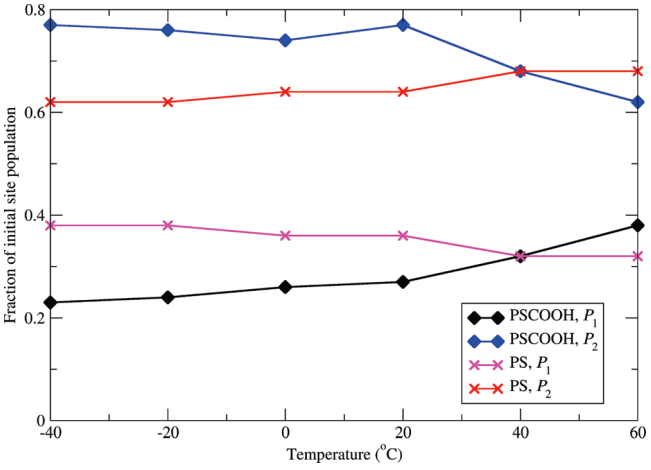

Figure 5. Initial site populations p_1 and p_2 as a function of temperature.

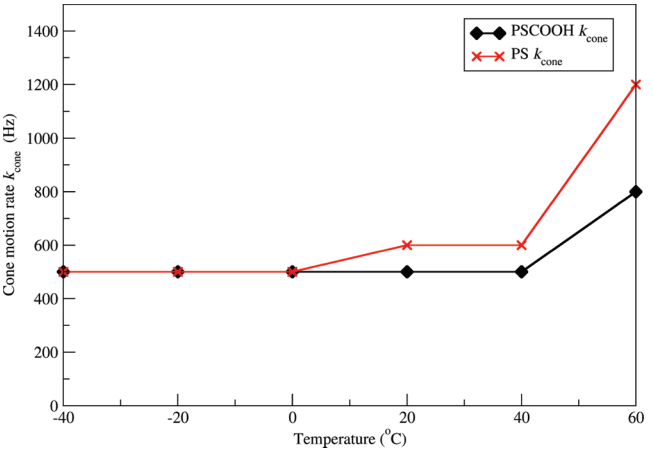

Figure 6. Cone motion rate, k_{cone}, as a function of temperature.

center of the spectrum in Figure 2a has a contribution from HDO, the simulation would not represent its presence at all. If the parameter set is adjusted to better match the central intensity of the quadrupolar echo spectrum, a best fit is obtained with parameter set 2. The resulting simulation appears in Figure 2b superimposed on the experimental spectrum. The two parameter sets have identical population ratios (p_1^{eq}/p_2^{eq} = 1/4) and rate constants for cone motion k_{cone}. The sets show small differences in the effective quadrupolar coupling constants and the cone half angles and a moderate difference in the side chain exchange rate, k_{12}. Although the simulation in Figure 2b shows improved agreement in the central portion of the spectrum, the agreement with data is still not perfect, and the fit to the outer portions of the spectrum is compromised. Because we have far more confidence in the data in outer portions of the spectrum where there is less interference from residual HDO, parameter set 1 is a better fit to the quadrupolar echo data, and it is a best fit to the MAS data.

Next, a ^{2}H MAS study was performed on the L8-deuterated LKα14 peptide adsorbed onto polystyrene (PS) and carboxylated polystyrene (PSCOOH) beads. ^{2}H MAS line shapes were obtained at temperatures of −40, −20, 0, 20, 40, and 60 °C, enabling a study of leucine side chain dynamics on PS and PSCOOH surfaces over a 100 °C temperature range. Representative experimental results, superimposed simulations, and the difference between simulation and experimental results are shown in Figure 4 for LKα14 on PS at T = 20 °C (4a), PSCOOH at T = 20 °C (4b), PS at T=−20 °C (4c), and PSCOOH at T=−20 °C (4d). Data and simulation sets for all other temperatures are provided as Supporting Information. All MAS line shape simulations were obtained using the model shown in Figure 2.

Trends in simulation parameters with temperature are shown in Figures 5 and 6 and Table 2. As shown in Figure 5, the site populations p_1 and p_2, which are associated with the exchange between the two dominant leucine side chain conformers, changed significantly throughout the temperature range studied on both PS and PSCOOH surfaces. Although the simulated line shapes were sensitive to the population ratio, they were substantially insensitive to the value of k_{12} over at least 3 orders of magnitude, which was therefore maintained at 3×10^6 s^{-1} for all fits. On PSCOOH surfaces at the lowest available temperature,

dx.doi.org/10.1021/jp1101829 |J. Phys. Chem. B 2011, 115, 9452–9460

Table 2. Simulation Parameters for All LK NMR Experiments

surface	temperature (°C)	QCC_{eff} (kHz)	k_{cone} (Hz)	p_1:p_2
PS	−40	49	500	0.38:0.62
PS	−20	48	500	0.38:0.62
PS	0	48	500	0.36:0.64
PS	20	46	600	0.36:0.64
PS	40	44	600	0.32:0.68
PS	60	45	1200	0.32:0.68
PSCOOH	−40	49	500	0.23:0.77
PSCOOH	−20	49	500	0.24:0.76
PSCOOH	0	48	500	0.26:0.74
PSCOOH	20	47	500	0.27:0.73
PSCOOH	40	44	500	0.32:0.68
PSCOOH	60	45	800	0.38:0.62
unbound	20	49	800	0.20:0.80

T = −40 °C, the a priori population ratio is $p_1^{eq}/p_2^{eq} \approx 3$. At ambient temperature (i.e., T = 20 °C), p_1^{eq}/p_2^{eq} has decreased to ∼2.5 on PSCOOH. This indicates the a priori populations of the dominant side chain conformers are somewhat less disparate in LKα14 bound to PSCOOH than in free LKα14 at ambient temperature, where according to Table 1, $p_1^{eq}/p_2^{eq} \approx 4$. As temperature increases, the difference between the site populations further decreases; p_1^{eq}/p_2^{eq} is ∼1.6 at T = 60 °C.

On PS surfaces the a priori populations are far less disparate than on PSCOOH for most of the temperature range of the study. For example, at T = −40 °C, the population ratio on PS is $p_1^{eq}/p_2^{eq} \approx 1.6$, compared with PSCOOH, where it is ∼3. But the most significant difference between side chain dynamics on PSCOOH versus PS is that whereas the population ratio decreases with temperature between −40 and 60 °C for PSCOOH, for PS, it remains largely unchanged from −40 and 20 °C, but then increases to ∼2.0 at T = 60 °C, which is slightly larger than the ratio of 1.6 on PSCOOH at the same temperature. The divergence of a priori population with increasing temperature indicates that the dynamics cannot be interpreted in terms of a conformational exchange in a constant potential where the site populations are governed by $p_1^{eq}/p_2^{eq} = e^{-\Delta E/kT}$, where $\Delta E = E_2 - E_1$ is the difference between the site energies. This issue will be discussed further below.

Trends in other dynamic parameters are similar for the two surfaces over most of the temperature range of the study. Table 2 shows that on both surfaces, the effective quadrupolar coupling constants diminishes slightly from around 49 kHz at T = −40 °C to 45 kHz at T = 60 °C. This trend possibly indicates the onset of additional fast, small amplitude motions as the temperature increases. The rate of diffusive motion of the peptide backbone on PS and PSCOOH is only ∼500 Hz at temperatures below 0 °C and, thus, makes only a minor contribution to the line shape at lower temperatures. Starting at T = 0 °C, the peptide motion on PS increases rapidly to over 1 kHz at T = 60 °C, whereas the rate of peptide motion remains constant on PSCOOH until T = 60 °C, where it increases slightly to 800 Hz.

MAS inversion recovery experiments were conducted on both surfaces at temperatures of −40, 20, and 50 °C. The results for the recovery time, T_1, are presented in Table 3.

The recovery time reaches a minimum when the rate constant for the correlation time, $R = 1/\tau_c$, is near to the Larmor frequency, ω_R. In this case, T_1 is increasing with temperature, putting this system well above the minimum T_1 at the measured temperatures; that is, $R \gg \omega_R$. In turn, this indicates that the fast motion of the methyl group rotation ($R_{CH_3} \sim 10^9$−10^{10} Hz) dominates the relaxation mechanism. Relaxation times on both surfaces are equivalent to within error, which is consistent with the above line shape analysis that identifies surface effects primarily from the slower conformational changes that are not observed in the T_1.

Table 3. Inversion Recovery Times As a Function of Temperature for L8-Deuterated LKα14 on PS and PSCOOH Surfaces

temperature (°C)	T_1 on PS (ms)	T_1 on PSCOOH (ms)
−40	24.8 ± 4.7	29.9 ± 3.3
20	54.7 ± 11.8	51.6 ± 8.0
50	77.6 ± 7.8	70.3 ± 4.6

DISCUSSION

Sum frequency generation vibrational spectroscopic studies of the LKα14 peptide system adsorbed onto planar PS indicate LKα14 adsorbs with the leucine face close to the PS surface.[15,16] Similar SFG studies of LKα14 adsorbed onto carboxylated SAMs on planar gold surfaces indicate the leucine face is oriented away from the carboxylated surface.[35] Static ^{2}H NMR line shape studies conducted at ambient temperature indicated that the primary impact of surface orientation is perturbation of the motion of the peptide main chain, which is rendered in our analysis as a diffusive cone motion of the entire leucine side chain. Specific motions internal to the leucine side chain itself (i.e., exchange between side chain conformers) vary at ambient temperature to a much lesser extent with surface orientation;[16] by contrast, static and MAS ^{2}H NMR studies reveal site-specific heterogeneity in both peptides[8,17] and porous bulk surfaces.[36] The present study seeks to further explore the fundamental origins of the surface dependence of the ^{2}H NMR line shape by specifically focusing upon the dependence of the ^{2}H MAS line shape of the CD_3 groups of L8 in LKα14 as a function of temperature and surface chemistry.

Ambient and physiological temperature (i.e., 30−40 °C) studies of LKα14 on PS and PSCOOH do not show a great variation in the p_1/p_2 ratio as a function of surface orientation. This fact is evident in Figure 5, which shows that the p_1 and p_2 curves for LKα14 on PS and PSCOOH intersect near 40 °C. What is clear in Figure 5 is the opposing trends for p_1 or p_2 versus temperature for the two surfaces. For LKα14 on PSCOOH, where the L8 side chain is directly opposite the surface, the a priori site populations converge as the temperature increases, whereas the same parameters diverge apparently for LKα14 on PS. The general dynamic trends with temperature for L8 on PSCOOH are observed in other leucyl peptides, in particular, the ^{2}H NMR study of the villin headpiece protein,[31] with increasing temperature correlated to a convergence in the initial site populations consistent with a straightforward Boltzmann population distribution, $p_1/p_2 = \exp(-(E_1-E_2/kT))$. This suggests a typical dynamic environment without unusual hindrances, as expected if the side chains are pointed away from the surface. The population ratio trend on the PS surface, however, remains fairly stable until diverging markedly at higher temperatures, 40−60 °C. This indicates an additional physical effect influencing the side chain dynamics at higher temperatures, such as a reorientation of the LK peptide as a whole. It is expected that the van der

Waals interaction between the nonpolar leucine side chains and PS surface is weaker than the electrostatic interaction between polar lysine side chain termini and surface-accessible carboxyl groups in the PSCOOH surface. At higher temperatures, the thermal energy of the LK peptide may be sufficient to overcome this binding interaction strength while remaining more constrained than the completely unbound peptide.

The sensitivity of leucine side chain dynamics to molecular environment is supported by an extensive literature. In particular, very sophisticated exploitations of the sensitivity of leucine side chain dynamics to local environment is found in membrane protein studies in which subtle aspects of the interaction between the protein and the lipid bilayer environment can be discerned from ^{2}H NMR line shapes of methyl-deuterated leucine side chains. For example, the transmembrane segment of phospholamban, which is believed to anchor the protein to the membrane, is rich in leucines. Analysis of ^{2}H NMR line shapes acquired for selectively leucine- and alanine-deuterated phospholambam in lipid bilayers have discerned the degree of insertion into the membrane,[7] helix packing interactions,[37] the mobility of a protein backbone hinge,[32] and the impact of single amino acid mutation on protein backbone motions.[38] A recent study of the lung surfactant peptide KL_4 by Long et al.[39] inferred from ^{2}H NMR spectra of selectively deuterated leucines the partitioning and orientation of KL_4 in DPPC/POPG and POPC/POPG phospholipid bilayers. From analysis of deuterated leucine side chain spectra, it was shown that KL_4 lies in the plane of the bilayers and adopts an unusual helical structure, which confers amphipathicity and allows partitioning into the lipid bilayer interior. One of the most quantitative of the ^{2}H NMR leucine studies is by Vugmeyster (discussed above), in which relaxation behavior is described by a phenomenological distribution of activation energies for CD_3 motions at high temperature, which collapses to a single distinctly smaller value at lower temperatures. Slower dynamics extracted by analysis of the line shape were attributed to diffusive motion of the peptide backbone and to exchange between the four unique side chain rotamers.

CONCLUSION

Surface-adsorbed proteins are perhaps the most challenging systems to be studied by solid state NMR. In contrast to crystalline proteins that are up to 50% protein by weight, NMR samples of surface-adsorbed proteins are less than 5% protein, assuming monolayer coverage is achieved. In practice, coverages lower than a monolayer are encountered. As a result, for the study of macromolecular surface dynamics with ^{2}H NMR, it is both desireable and necessary to use deuterium MAS methods. Here, we have not only acquired high quality deuterium MAS spectra from samples of selectively deuterated surface-adsorbed proteins but also shown that these MAS line shapes can be quantified in terms of specific models of amino acid side chain motions and that these dynamics are indicative of surface proximity. The present study demonstrates these ^{2}H MAS approaches applied to samples of surface-adsorbed deuterated leucyl peptides, which have high deuterium content and relatively narrow lines and, thus, can also be studied using static ^{2}H NMR line shape analysis. In the future, we will show how ^{2}H MAS makes possible the detection of line shapes that are much broader than shown here; namely, phenylalanine side chains attached to surface-adsorbed proteins.

ASSOCIATED CONTENT

Supporting Information. Complete MAS line shapes for all temperatures, details of sideband intensities, inversion recovery intensities and fits, and a comparison of simulation to experimental data for the model compound dimethylsulfone-d_6. This material is available free of charge via the Internet at http://pubs.acs.org.

AUTHOR INFORMATION

Corresponding Author

*Phone: (206) 685-2052. Fax: (206) 685-8665. E-mail: drobny@chem.washington.edu.

Present Addresses

[§]Department of Chemical Physics, Weizmann Institute of Science, Rehovot, 76100 Israel

ACKNOWLEDGMENT

The authors acknowledge support from NIH R01 GM074511 and R01 DE12554.

REFERENCES

(1) Barnes, R. G. Deuteron quadrupole coupling tensors in solids. In *Advances in Nuclear Quadrupole Resonance*; Smith, J. A. S., Ed.; Heyden: London, 1974; Vol. 1; pp 335−355.
(2) Auger, M.; Smith, I. C.; Jarrell, H. C. *Biophys. J.* **1991**, *59*, 31–38.
(3) Lorieau, J. L.; McDermott, A. E. *J. Am. Chem. Soc.* **2006**, *128*, 11505–11512.
(4) Hansen, A. L.; Al-Hashimi, H. M. *J. Am. Chem. Soc.* **2007**, *129*, 16072–16082.
(5) Zhang, Q.; Stelzer, A. C.; Fisher, C. K.; Al-Hashimi, H. M. *Nature* **2007**, *450*, 1263–1267.
(6) Olsen, G. L.; Echodu, D. C.; Shajani, Z.; Bardaro, M. F.; Varani, G.; Drobny, G. P. *J. Am. Chem. Soc.* **2008**, *130*, 2896–2897.
(7) Tiburu, E. K.; Karp, E. S.; Dave, P. C.; Damodaran, K.; Lorigan, G. A. *Biochemistry* **2004**, *43*, 13899–13909.
(8) Breen, N. F.; Weidner, T.; Li, K.; Castner, D. G.; Drobny, G. P. *J. Am. Chem. Soc.* **2009**, *131*, 14148–14149.
(9) Glaubitz, C.; Burnett, I. J.; Gröbner, G.; Mason, A. J.; Watts, A. *J. Am. Chem. Soc.* **1999**, *121*, 5787–5794.
(10) Lee, H.; Ortiz de Montellano, P. R.; McDermott, A. E. *Biochemistry* **1999**, *38*, 10808–10813.
(11) Agarwal, V.; Faelber, K.; Schmieder, P.; Reif, B. *J. Am. Chem. Soc.* **2008**, *131*, 2–3.
(12) Vold, R. L.; Hoatson, G. L. *J. Magn. Reson.* **2009**, *198*, 57–72.
(13) DeGrado, W. F.; Lear, J. D. *J. Am. Chem. Soc.* **1985**, *107*, 7684–7689.
(14) Long, J. R.; Oyler, N.; Drobny, G. P.; Stayton, P. S. *J. Am. Chem. Soc.* **2002**, *124*, 6297–6303.
(15) Mermut, O.; Phillips, D. C.; York, R. L.; McCrea, K. R.; Ward, R. S.; Somorjai, G. A. *J. Am. Chem. Soc.* **2006**, *128*, 3598–3607.
(16) Phillips, D. C.; York, R. L.; Mermut, O.; McCrea, K. R.; Ward, R. S.; Somorjai, G. A. *J. Phys. Chem. C* **2007**, *111*, 255–261.
(17) Weidner, T.; Breen, N. F.; Li, K.; Drobny, G. P.; Castner, D. G. *Proc. Natl. Acad. Sci.* **2010**, *107*, 13288–13293.
(18) Atherton, E.; Sheppard, R. C. *Solid phase peptide synthesis: a practical approach*; Oxford University Press: Oxford, 1989.
(19) Davis, J. H. *Biophys. J.* **1979**, *27*, 339–358.
(20) Spiess, H. W.; Sillescu, H. *J. Magn. Reson.* **1981**, *42*, 381–389.
(21) Wittebort, R. J.; Olejniczak, E. T.; Griffin, R. G. *J. Chem. Phys.* **1987**, *86*, 5411–5420.
(22) Lin, T. H.; Vold, R. R.; Vold, R. L. *J. Magn. Reson.* **1991**, *95*, 71–79.

(23) Magnus, W.; Winkler, S. Floquet's Theorem. In *Hill's Equation*; Dover: New York, 1979; pp 3−8.
(24) Weintraub, O.; Vega, S. *J. Magn. Reson., Series A* **1993**, *105*, 245–267.
(25) Duer, M. J.; Levitt, M. H. *Solid State Nucl. Magn. Reson.* **1992**, *1*, 211–215.
(26) Torchia, D. A.; Szabo, A. *J. Magn. Reson.* **1982**, *49*, 107–121.
(27) Abragam, A. *The Principles of Nuclear Magnetism*; Oxford University Press: Oxford, 1961.
(28) Batchelder, L. S.; Sullivan, C. E.; Jelinski, L. W.; Torchia, D. A. *Proc. Natl. Acad. Sci. Biol.* **1982**, *79*, 386–389.
(29) Hologne, M.; Faelber, K.; Diehl, A.; Reif, B. *J. Am. Chem. Soc.* **2005**, *127*, 11208–11209.
(30) Hologne, M.; Chen, Z. J.; Reif, B. *J. Magn. Reson.* **2006**, *179*, 20–28.
(31) Vugmeyster, L.; Ostrovsky, D.; Ford, J. J.; Burton, S. D.; Lipton, A. S.; Hoatson, G. L.; Vold, R. L. *J. Am. Chem. Soc.* **2009**, *131*, 13651–13658.
(32) Abu-Baker, S.; Lu, J. X.; Chu, S. D.; Brinn, C. C.; Makaroff, C. A.; Lorigan, G. A. *Biochemistry* **2007**, *46*, 11695–11706.
(33) Benedetti, C. In *Proceedings of the Fifth American Peptides Symposium*; Goodman, M., Meienhofer, J., Eds.; Wiley: New York, 1977; pp 257−274.
(34) Janin, J.; Wodak, S.; Levitt, M.; Maigret, B. *J. Mol. Biol.* **1978**, *125*, 357–386.
(35) Weidner, T.; Apte, J. S.; Gamble, L. J.; Castner, D. G. *Langmuir* **2010**, *26*, 3433–3440.
(36) Gath, J.; Hoaston, G. L.; Vold, R. L.; Berthoud, R.; Coperet, C.; Grellier, M.; Sabo-Etienne, S.; Lesage, A.; Emsley, L. *Phys. Chem. Chem. Phys.* **2009**, *11*, 6962–6971.
(37) Ying, W. W.; Irvine, S. E.; Beekman, R. A.; Siminovitch, D. J.; Smith, S. O. *J. Am. Chem. Soc.* **2000**, *122*, 11125–11128.
(38) Chu, S.; Coey, A. T.; Lorigan, G. A. *Biochim. Biophys. Acta, Biomembr.* **2010**, *1798*, 210–215.
(39) Long, J. R.; Mills, F. D.; Ganesh, O. K.; Antharam, V. C.; Farver, R. S. *Biochim. Biophys. Acta, Biomembr.* **2010**, *1798*, 216–222.